Multilayered Functionally Graded Non-linear Elastic Beams with Logarithmic Material Gradient: A Delamination Analysis

V. Rizov

The delamination fracture in a multilayered functionally graded cantilever beam configuration that exhibits material non-linearity is analyzed in terms of the strain energy release rate. The beam under consideration has an arbitrary number of adhesively bonded horizontal layers of different thicknesses and material properties. The delamination crack is located arbitrary along the beam height. The material non-linearity is described by a stress-strain relation that involves two material properties. It is assumed that the two material properties are functionally graded in both width and thickness directions in each layer. Logarithmic laws are used to describe the variation of the material properties in the cross-sections of the layers (the material properties are distributed non-symmetrically with respect to the centroidal axes of the beam cross-section). The balance of the energy is analyzed in order to derive the strain energy release rate. The J-integral approach is applied for verification. Parametric investigations are carried-out in order to evaluate the influence of the gradients of the two material properties in both width and thickness directions of the layers on the delamintion fracture behaviour. The results obtained show that the strain energy release rate can be controlled by using appropriate material gradients in the design stage of multilayered functionally graded structural members exhibiting material non-linearity.

1 Introduction

Since the material properties of functionally graded materials vary gradually along one or more spatial coordinates, the behaviour of structural members and components made of these novel inhomogeneous materials can be modified to meet various performance requirements. Thus, it is not surprising that recently, the international academic circles have paid significant attention to the development of functionally graded materials and their applications in different structural members, components and devices (Bykov et al., 2012; Gasik, 2010; Hirai and Chen, 1999; Mortensen and Suresh, 1995; Nemat-Allal et al., 2011; Neubrand and Rödel, 1997; Suresh and Mortensen, 1998; Uslu Uysal and Kremzer, 2015; Uslu Uysal, 2016). However, the integrity of these structural members and components depends to a great extent on their fracture performance. Therefore, fracture in functionally graded materials is a subject worth to explore (Upadhyay and Simha, 2007; Yan and Yang, 2011; Uslu Uysal and Güven, 2016).

Cracked functionally graded beam configurations have been investigated by Upadhyay and Simha, 2007. Fracture analyses of beams loaded in three-point bending have been developed assuming linear-elastic behaviour of the functionally graded material. The compliance approach for evaluation of beams containing crack have been explored. Equivalent homogeneous beams of variable height for cracked beams have been developed by using methods of linear-elastic fracture mechanics. It has been shown that the equivalent beam captures the compliance characteristics of the cracked functionally graded beam with good accuracy. It has been found that besides for three-point bending beams, the method is suitable also for analyzing cracked functionally graded components loaded in bending by concentrated loads.

Analyses of slender functionally graded beams with open edge cracks have been carried-out by Yan and Yang, 2011. The cracked sections have been modelled by rotational mass-less spring. Methods of linear-elastic fracture mechanics have been applied. Dynamic behaviour of cracked cantilever, hinged-hinged and clamped-clamped functionally graded linear-elastic beams has been studied analytically. It has been assumed that the beams are

functionally graded in the height direction. Effects of the location and the number of cracks, the external loading and the boundary conditions on the fracture behaviour have been elucidated.

Interesting analyses of structural members in the presence of inhomogeneties, defects and cracks by applying engineering-type theories of bars, beams, shafts, discs, plates and shells have been developed by Kienzler and Herrmann, 2001; Kienzler and Bose, 2008; Schneider and Kienzler, 2011.

Multilayered materials are a promising class of inhomogeneous structural materials which are characterized by high strength-to-weight and stiffness-to-weight ratios. Multilayered materials play an important role in various engineering applications in aeronautics, automotive industries and infrastructure. The reliability and integrity of layered structures is closely related with their delamination fracture behaviour (Dolgov, 2005; Dolgov, 2016; Szekrenyes, 2016; Szekrenyes, 2016; Rizov, 2017).

A non-linear analytical solution for the strain energy release rate in the multilayered functionally graded Split Cantilever Beam configuration has been derived by Rizov, 2017. The beam has been made of an arbitrary number of longitudinal vertical layers. A delamination crack has been located arbitrary along the width of the beam cross-section. It has been assumed that the material is functionally graded in the thickness directions of each layer (i.e., the material is one dimensional functionally graded). The non-linear behaviour of the functionally graded material has been described by a power-law stress-strain relation.

The present paper is focussed on a delamination fracture analysis of a multilayered functionally graded cantilever beam configuration with considering the non-linear mechanical behaviour of the material. It is assumed that the two material properties which are involved in the non-linear stress-strain relation are functionally graded in both thickness and width directions in each layer (i.e., the material is two-dimensional functionally graded). Logarithmic laws are applied to describe the continuous variation of the two material properties in the cross-sections of the layers (the properties are distributed non-symmetrically with respect to the centroidal axes of the beam cross-section). An approach for determination of the bending moments in the two crack arms is developed. The solution for the strain energy release rate obtained by considering the balance of the energy is used to analyze the influence of material gradients in both thickness and width directions, the delamination crack location and the material non-linearity on the delamination fracture behaviour.

2   Solution for the Strain Energy Release Rate

The cantilever beam configuration, shown in Fig. 1, is made by an arbitrary number of adhesively bonded horizontal layers. The beam is clamped in section, B.
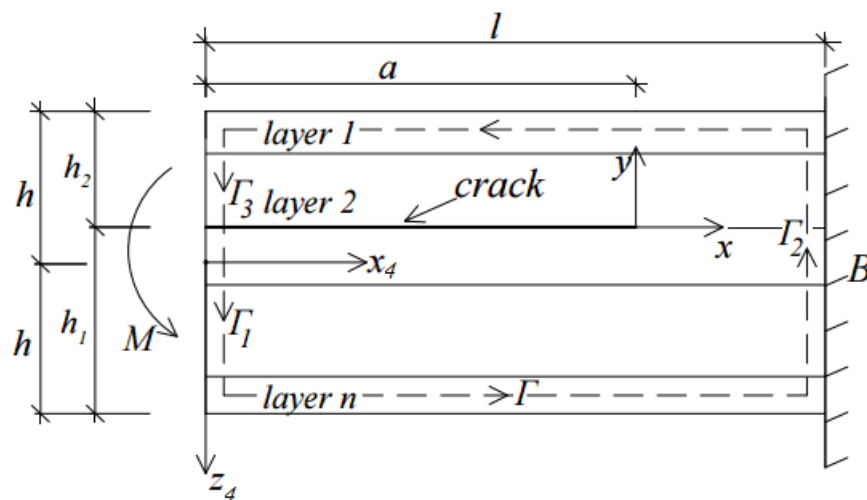

Figure 1: Schematic of multilayered functionally graded cantilever beam containing a delamination crack

It is assumed that each layer has individual thickness and material properties. Also, the material in each layer is functionally graded in both thickness and width directions of the layer. Besides, the material exhibits non-linear

mechanical behaviour. The beam cross-section is a rectangle of width, b, and height, $2h$. The beam length is l. The external loading consists of one moment, M, applied at the free end of the beam. A delamination crack of length, a, is located arbitrary between layers. The thicknesses of the lower and upper crack arms are h_1 and h_2, respectively.

In the present paper, the delamination is analyzed in terms of the strain energy release rate, G, by considering the balance of the energy. For this purpose, the balance of the energy is written as

$$M\delta\varphi = \frac{\partial U}{\partial a}\delta a + Gb\delta a \,, \tag{1}$$

where $\delta\varphi$ is the increase of the rotation of the beam free end induced by an increase of the crack length, δa. In (1), U is the strain energy. From (1), G is expressed as

$$G = \frac{M}{b}\frac{\partial\varphi}{\partial a} - \frac{1}{b}\frac{\partial U}{\partial a} \,. \tag{2}$$

It should be noted that the present analysis is based on the small strains hypothesis.
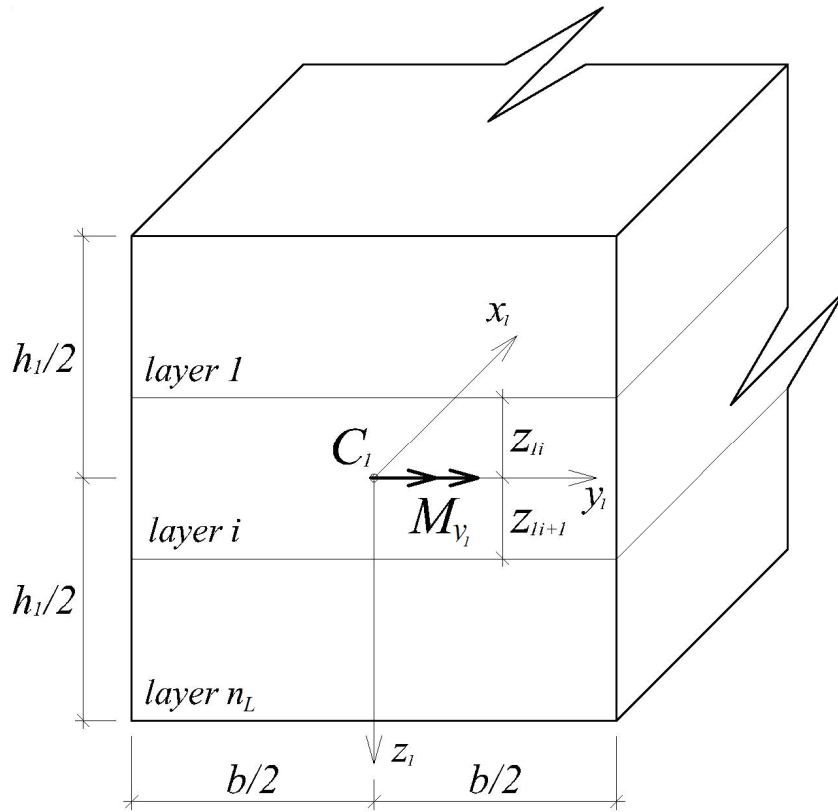

Figure 2: The geometry and loading of the free end of the lower crack arm

The rotation, φ, of the beam free end is obtained by applying the Castigliano's theorem for structures exhibiting material non-linearity

$$\varphi = \frac{\partial U^*}{\partial M} \,, \tag{3}$$

where U^* is the complementary strain energy.

The complementary strain energy, cumulated in the beam, is obtained as

$$U^* = U_L^* + U_U^* + U_R^*,$$ (4)

where U_L^*, U_U^* and U_R^* are, respectively, the complementary strain energies in the lower crack arm, the upper crack arm and the un-cracked beam portion, $a \le x_4 \le l$, (Fig. 1).

The complementary strain energy in the lower crack arm is expressed as

$$U_L^* = a \sum_{i=1}^{i=n_L} \int_{-\frac{b}{2}}^{\frac{b}{2}} \int_{z_{1i}}^{z_{1i+1}} u_{0L_i}^* dy_1 dz_1,$$ (5)

where n_L is the number of layers in the lower crack arm, z_{1i} and z_{1i+1} are, respectively, the coordinates of the upper and lower surfaces of the i-th layer (Fig. 2), $u_{0L_i}^*$ is the complementary strain energy density in the same layer, y_1 and z_1 are the centroidal axes.
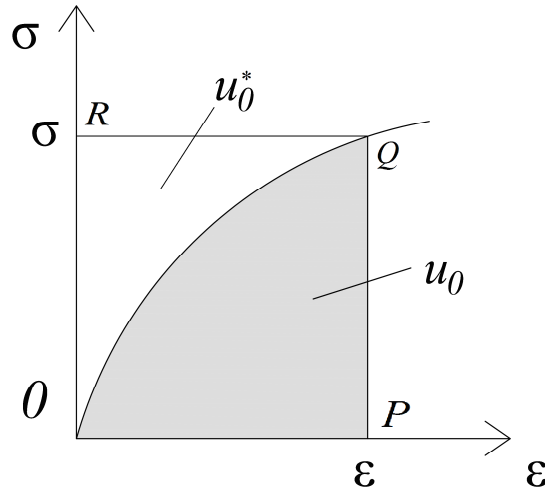

Figure 3: Non-linear stress-strain curve (the strain energy and the complementary strain energy densities are denoted by u_0 and u_0^*, respectively)

The complementary strain energy density is equal to the area, OQR, which supplements the area, OPQ, enclosed by the stress-strain curve to a rectangle (Fig. 3). Thus, $u_{0L_i}^*$ is written as

$$u_{0L_i}^* = \sigma_i \varepsilon - u_{0L_i},$$ (6)

where σ_i is the distribution of the longitudinal normal stresses in the i-th layer of the lower crack arm, u_{0L_i} is the strain energy density in the same layer, ε is the distribution of the longitudinal strains. The strain energy density is equal to the area, OPQ, enclosed by the stress-strain curve (Fig. 3). Therefore, u_{0L_i} is expressed as

$$u_{0L_i} = \int_0^\varepsilon \sigma_i d\varepsilon.$$ (7)

The present analysis uses the following non-linear stress-strain relation (Lukash, 1998):

$$\sigma_i = \frac{\varepsilon}{q_i + r_i \varepsilon},$$

(8)

where q_i and r_i are material properties in the i-th layer.

From (7) and (8), one derives

$$u_{0L_i} = \frac{1}{r_i}\left[\varepsilon - \beta_i \ln(\varepsilon + \beta_i) + \beta_i \ln(\beta_i)\right],$$

(9)

where

$$\beta_i = \frac{q_i}{r_i}.$$

(10)

From (6), (8) and (9), one obtains

$$u_{0L_i}^* = \frac{\varepsilon^2}{q_i + r_i \varepsilon} - \frac{\varepsilon}{r_i} + \frac{\beta_i}{r_i}\ln(\varepsilon + \beta_i) - \frac{\beta_i}{r_i}\ln\beta_i.$$

(11)

It is assumed that q_i and r_i vary continuously in the cross-section of the i-th layer according to the following logarithmic laws:

$$q_i = q_{0_i} \ln\left(e + p_{q_i}\frac{y_1 + \frac{b}{2}}{b} + m_{q_i}\frac{z_1 - z_{1i}}{z_{1i+1} - z_{1i}}\right),$$

(12)

$$r_i = r_{0_i} \ln\left(e + p_{r_i}\frac{y_1 + \frac{b}{2}}{b} + m_{r_i}\frac{z_1 - z_{1i}}{z_{1i+1} - z_{1i}}\right),$$

(13)

where q_{0_i}, p_{q_i}, m_{q_i}, r_{0_i}, p_{r_i} and m_{r_i} are material properties. In (12) and (13), y_1 and z_1 vary in the intervals $\left[-b/2; b/2\right]$ and $\left[z_{1i}; z_{1i+1}\right]$, respectively. The gradients of q_i in width and thickness directions of the i-th layer are governed by p_{q_i} and m_{q_i}, respectively. The material properties, p_{r_i} and m_{r_i}, control the gradients of r_i in the in width and thickness directions of the i-th layer, respectively. Formulae (12) and (13) show that q_i and r_i are distributed non-symmetrically with respect to y_1 and z_1.

The distribution of the longitudinal strains is analyzed by applying the Bernoulli's hypothesis for plane sections since the span to height ratio of the beam under consideration is large. It should also be noted that since the beam is loaded in pure bending, the only non-zero strain is ε. Thus, according to the small strains compatibility equations, ε is distributed linearly in the cross-section. Hence, the strain distribution in the cross-section of the left-hand crack arm is written as

$$\varepsilon = \varepsilon_{C_1} + \kappa_{y_1} y_1 + \kappa_{z_1} z_1, \tag{14}$$

where ε_{C_1} is the strain in the centre of the cross-section, κ_{y_1} and κ_{z_1} are the curvatures of lower crack arm in the $x_1 y_1$ and $x_1 z_1$ planes, respectively. Concerning the aplicability of the Bernoulli's hypothesis for plane sections, it sholud be mentioned that this hypothesis has already been used by other authors in fracture analyses of inhomogeneous structural members, such as functionally graded beams (Upadhyay and Simha, 2007), multilayered beams (Hsueh et al., 2009) and composite beams (Farris and Doyle, 1991).

The quantities, ε_{C_1}, κ_{y_1} and κ_{z_1}, are determined in the following manner. First, three equations are derived by using the conditions for equilibrium of the elementary forces in the cross-section of the lower crack arm

$$N_1 = \sum_{i=1}^{i=n_L} \iint_{A_i} \sigma_i dA_i, \tag{15}$$

$$M_{y_1} = \sum_{i=1}^{i=n_L} \iint_{A_i} \sigma_i z_1 dA_i, \tag{16}$$

$$M_{z_1} = \sum_{i=1}^{i=n_L} \iint_{A_i} \sigma_i y_1 dA_i, \tag{17}$$

where N_1 is the axial force, M_{y_1} and M_{z_1} are and bending moments about y_1 and z_1 axes, respectively. One can observe in Fig. 2 that

$$N_1 = 0, \ M_{z_1} = 0. \tag{18}$$

By combining of (8), (12), (13), (14), (15), (16) and (17), one obtains

$$N_1 = \sum_{i=1}^{i=n_L} \left(f_i \mu_i + \frac{1}{2} g_i \nu_i + \frac{1}{3} c_i \zeta_i \right), \tag{19}$$

$$M_{y_1} = \sum_{i=1}^{i=n_L} \left[\frac{1}{2} f_i \nu_i + \frac{1}{3} g_i \zeta_i + \frac{1}{4} c_i \left(z_{1i+1}^4 - z_{1i}^4 \right) \right], \tag{20}$$

$$M_{z_1} = \frac{b^3}{12} \sum_{i=1}^{i=n_L} \left[\left(\varepsilon_{C_1} \phi_i + \kappa_{y_1} \lambda_i \right) \mu_i + \frac{1}{2} \left(\kappa_{y_1} \theta_i + \kappa_{z_1} \phi_i \right) \nu_i \right], \tag{21}$$

$$\beta_i = e + \frac{p_{q_i}}{2} - \frac{m_{q_i} z_{1i}}{z_{1i+1} - z_{1i}}, \tag{22}$$

$$\delta_i = \frac{p_{q_i}}{b}, \tag{23}$$

$$\varphi_i = \frac{m_{q_i}}{z_{1i+1} - z_{1i}}, \tag{24}$$

$$\eta_i = \frac{p_{q_i}}{2},\tag{25}$$

$$\omega_i = e + \frac{p_{r_i}}{2} - \frac{m_{r_i} z_{1i}}{z_{1i+1} - z_{1i}},\tag{26}$$

$$\psi_i = \frac{m_{r_i}}{z_{1i+1} - z_{1i}},\tag{27}$$

$$\gamma_i = q_{0_i} \ln \beta_i + r_{0_i} \varepsilon_{C_1} \ln \omega_i,\tag{28}$$

$$\phi_i = -\frac{1}{\gamma_i^2}\left(\frac{q_{0_i}\delta_i}{\beta_i} + \frac{r_{0_i}\eta_i\varepsilon_{C_1}}{\omega_i} + r_{0_i}\kappa_{y_1} \ln \omega_i\right),\tag{29}$$

$$\theta_i = -\frac{1}{\gamma_i^2}\left(\frac{q_{0_i}\varphi_i}{\beta_i} + \frac{r_{0_i}\psi_i\varepsilon_{C_1}}{\omega_i} + r_{0_i}\kappa_{z_1} \ln \omega_i\right),\tag{30}$$

$$\mu_i = z_{1i+1} - z_{1i},\tag{31}$$

$$\nu_i = z_{1i+1}^2 - z_{1i}^2,\tag{32}$$

$$\zeta_i = z_{1i+1}^3 - z_{1i}^3,\tag{33}$$

$$\lambda_i = \frac{1}{\gamma_i},\tag{34}$$

$$f_i = b\left(\varepsilon_{C_1}\lambda_i + \frac{1}{12}\kappa_{y_1}\phi_i b^2\right),\tag{35}$$

$$g_i = b\left(\varepsilon_{C_1}\theta_i + \kappa_{z_1}\lambda_i\right),\tag{36}$$

$$c_i = b\kappa_{z_1}\theta_i.\tag{37}$$

It should be noted that at $n_L = 1$, $p_{q_i} = 0$, $m_{q_i} = 0$, $r_{0_i} = 1$, $p_{r_i} = 0$ and $m_{r_i} = 0$, equations (19), (20) and (21) transform in

$$N_1 = \varepsilon_{C_1} \frac{1}{q_{0_i}} bh_1,\tag{38}$$

$$M_{y_1} = \frac{bh_1^3}{12} \frac{1}{q_{0_i}} \kappa_{z_1},\tag{39}$$

$$M_{z_1} = \frac{b^3 h_1}{12} \frac{1}{q_{0_i}} \kappa_{y_1}.\tag{40}$$

It is obvious that (38), (39) and (40) coincide with equations for equilibrium of linear-elastic homogeneous beam of rectangular cross-section of width, b_1, and height, h_1, (Dowling, 2007). This fact is an indication for the consistency of equations (19), (20) and (21) since at $r_i = 0$ the non-linear stress-strain relation (8) transforms into the Hooke's law assuming that $1/q_{0_i}$ is the modulus of elasticity.

There are four un-knows, ε_{C_1}, κ_{y_1}, κ_{z_1} and M_{y_1}, in equations (19), (20) and (21). The fact that the two crack arms deform with the same curvature in the $x_4 z_4$ plane (Fig.1), gives us the following condition

$$\kappa_{z_2} = \kappa_{z_1}, \tag{41}$$

where κ_{z_2} is the curvature of the upper crack arm in the $x_2 z_2$ plane (z_2 is the vertical centroidal axis of the cross-section of the upper crack arm).

Also, it is obvious that

$$M_{y_1} + M_{y_2} = M, \tag{42}$$

where M_{y_2} is the bending moment about the horizontal centroidal axis, y_2, of the cross-section of the upper crack arm.

By using (19), (20), (21), (41) and (42), the equations for equilibrium of the cross-section of the upper-crack arm are written as

$$N_2 = \sum_{i=1}^{i=n_U} \left(f_{U_i} \mu_{U_i} + \frac{1}{2} g_{U_i} v_{U_i} + \frac{1}{3} c_{U_i} \zeta_{U_i} \right), \tag{43}$$

$$M - M_{y_1} = \sum_{i=1}^{i=n_U} \left[\frac{1}{2} f_{U_i} v_{U_i} + \frac{1}{3} g_{U_i} \zeta_{U_i} + \frac{1}{4} c_{U_i} \left(z_{2i+1}^4 - z_{2i}^4 \right) \right], \tag{44}$$

$$M_{z_2} = \frac{b^3}{12} \sum_{i=1}^{i=n_U} \left[\left(\varepsilon_{C_2} \phi_{U_i} + \kappa_{y_2} \lambda_{U_i} \right) \mu_{U_i} + \frac{1}{2} \left(\kappa_{y_2} \theta_{U_i} + \kappa_{z_1} \phi_{U_i} \right) v_{U_i} \right], \tag{45}$$

where n_U is the number of layers in the upper crack arm, N_2 and M_{z_2} are, respectively, the axial force and the bending moment about z_2 axis (apparently, $N_2 = 0$ and $M_{z_2} = 0$), z_{2i} are z_{2i+1} are, respectively, the coordinates of the upper and lower surface of the i-th layer in the upper crack arm, ε_{C_2} is the strain in the centre of the cross-section of the upper crack arm, κ_{y_2} is the curvature of the upper crack arm in the $x_2 y_2$ plane . The quantities, β_{U_i}, δ_{U_i}, φ_{U_i}, η_{U_i}, ω_{U_i}, ψ_{U_i}, γ_{U_i}, ϕ_{U_i}, θ_{U_i}, μ_{U_i}, v_{U_i}, ζ_{U_i}, λ_{U_i}, f_{U_i}, g_{U_i} and c_{U_i} are determined by formulae (22) – (37). For this purpose, z_{1i}, z_{1i+1}, ε_{C_1} and κ_{y_1} are replaced with z_{2i}, z_{2i+1}, ε_{C_2} and κ_{y_2}, respectively.

Equations (19), (20), (21), (43), (44) and (45) should be solved with respect to ε_{C_1}, κ_{y_1}, κ_{z_1}, ε_{C_2}, κ_{y_2} and M_{y_1} by using the Matlab computer program.

The complementary strain energy cumulated in the upper crack arm is expressed as

$$U_U^* = a \sum_{i=1}^{i=n_U} \int_{-\frac{b}{2}}^{\frac{b}{2}} \int_{z_{2i}}^{z_{2i+1}} u_{0U_i}^* \, dy_2 dz_2 \,,\tag{46}$$

where the complementary strain energy density, $u_{0U_i}^*$, in the i-th layer of the upper crack arm is obtained by (11). For this purpose, ε is replaced with ε_U. The distribution of the longitudinal strains, ε_U, in the cross-section of the upper crack arm is obtained by (14) by replacing of ε, ε_{C_1}, κ_{y_1}, κ_{z_1}, y_1 and z_1 with ε_U, ε_{C_2}, κ_{y_2}, κ_{z_2}, y_2 and z_2, respectively.

The complementary strain energy cumulated in the un-cracked beam portion is written as

$$U_R^* = a \sum_{i=1}^{i=n} \int_{-\frac{b}{2}}^{\frac{b}{2}} \int_{z_{3i}}^{z_{3i+1}} u_{0R_i}^* \, dy_3 dz_3 \,,\tag{47}$$

where n is the number of the layers in the un-cracked beam portion, z_{3i} and z_{3i+1} are, respectively, the coordinates of the upper and lower surfaces of the i-th layer, $u_{0R_i}^*$ is the complementary strain energy density in the same layer, y_3 and z_3 are the centroidal axes of the cross-section of the un-cracked beam portion.

Formula (11) is applied to obtain $u_{0R_i}^*$. For this purpose, ε is replaced with ε_R. Formula (14) is used to obtain the distribution of the longitudinal strains, ε_R, in the cross-section of the un-cracked beam portion. For this purpose, ε, ε_{C_1}, κ_{y_1}, κ_{z_1}, y_1 and z_1 are replaced with ε_R, ε_{C_3}, κ_{y_3}, κ_{z_3}, y_3 and z_3, respectively. Here, ε_{C_3} is the longitudinal strain in the centre of the cross-section of the un-cracked beam portion, κ_{y_3} and κ_{z_3} are the curvatures of the un-cracked beam portion, respectively, in the $x_3 y_3$ and $x_3 z_3$ planes, y_3 and z_3 are the centroidal axes of the cross-section of the un-cracked beam portion. Equations (19), (20) and (21) are used to determine ε_{C_3}, κ_{y_3} and κ_{z_3}. For this purpose, N_1, M_{y_1}, M_{z_1}, n_L, z_{1i}, z_{1i+1}, ε_{C_1}, κ_{y_1} and κ_{z_1} are replaced, respectively, with N_3, M_{y_3}, M_{z_3}, n, z_{3i}, z_{3i+1}, ε_{C_3}, κ_{y_3} and κ_{z_3} in formulae (19) – (37). It is obvious that $N_1 = 0$, $M_{y_1} = M$ and $M_{z_1} = 0$.

The strain energy cumulated in the beam is expressed as

$$U = U_L + U_U + U_R \,,\tag{48}$$

where U_L, U_U and U_R are the strain energies in the lower crack arm, the upper crack arm and the un-cracked beam portion, respectively.

U_L is written as

$$U_L = a \sum_{i=1}^{i=n_L} \int_{-\frac{b}{2}}^{\frac{b}{2}} \int_{z_{1i}}^{z_{1i+1}} u_{0L_i} \, dy_1 dz_1 \,,\tag{49}$$

where u_{0L_i} is obtained by formula (9).

The strain energy cumulated in the upper crack arm is expressed as

$$U_U = a \sum_{i=1}^{i=n_U} \int_{-\frac{b}{2}}^{\frac{b}{2}} \int_{z_{2i}}^{z_{2i+1}} u_{0U_i} \, dy_2 dz_2 \, .$$

(50)

Formula (9) is applied to obtain u_{0U_i}. For this purpose, ε is replaced with ε_U .

The strain energy in the un-cracked beam portion is written as

$$U_R = a \sum_{i=1}^{i=n} \int_{-\frac{b}{2}}^{\frac{b}{2}} \int_{z_{3i}}^{z_{3i+1}} u_{0R} \, dy_3 dz_3 \, ,$$

(51)

where u_{0R_i} is determined by (9) by replacing of ε with ε_R .

Finally, by substituting of (3), (4), (5), (46), (47), (48), (49), (50) and (51) in (2), one obtains

$$G = \frac{M}{b} \frac{\partial}{\partial M} \left(\sum_{i=1}^{i=n_L} \int_{-\frac{b}{2}}^{\frac{b}{2}} \int_{z_{1i}}^{z_{1i+1}} u_{0L_i}^* \, dy_1 dz_1 + \sum_{i=1}^{i=n_U} \int_{-\frac{b}{2}}^{\frac{b}{2}} \int_{z_{2i}}^{z_{2i+1}} u_{0U_i}^* \, dy_2 dz_2 - \sum_{i=1}^{i=n} \int_{-\frac{b}{2}}^{\frac{b}{2}} \int_{z_{3i}}^{z_{3i+1}} u_{0R_i}^* \, dy_3 dz_3 \right) -$$

$$- \frac{1}{b} \left(\sum_{i=1}^{i=n_L} \int_{-\frac{b}{2}}^{\frac{b}{2}} \int_{z_{1i}}^{z_{1i+1}} u_{0L_i} \, dy_1 dz_1 + \sum_{i=1}^{i=n_U} \int_{-\frac{b}{2}}^{\frac{b}{2}} \int_{z_{2i}}^{z_{2i+1}} u_{0U_i} \, dy_2 dz_2 - \sum_{i=1}^{i=n} \int_{-\frac{b}{2}}^{\frac{b}{2}} \int_{z_{3i}}^{z_{3i+1}} u_{0R_i} \, dy_3 dz_3 \right).$$

(52)

The integration in (52) should be performed by the MatLab computer program. The derivative, $\frac{\partial}{\partial M}(...)$, in (52) should be determined numerically by the MatLab computer program.

The solution for the strain energy release rate (52) is verified by the *J*-integral approach (Broek, 1986). The *J*-integral is solved along the integration contour, Γ, shown by a dashed line in Fig.1. Since the *J*-integral has non-zero values only in segments, Γ_1, Γ_2 and Γ_3, of the integration contour, the *J*-integral solution is written as

$$J = J_{\Gamma_1} + J_{\Gamma_2} + J_{\Gamma_3} \, ,$$

(53)

where J_{Γ_1}, J_{Γ_2} and J_{Γ_3} are the values of the *J*-integral in segments Γ_1, Γ_2 and Γ_3, respectively (Γ_1 and Γ_3 coincide, respectively, with the cross-sections of the lower and upper crack arms, Γ_2 coincides with the clamping).

First, the integration is performed in segment, Γ_1. The *J*-integral is written as

$$J_{\Gamma_1} = \sum_{i=1}^{i=n_L} \int_{z_{1i}}^{z_{1i+1}} \left[u_{0L_i} \cos\alpha - \left(p_{x_i} \frac{\partial u}{\partial x} + p_{y_i} \frac{\partial v}{\partial x} \right) \right] ds \, ,$$

(54)

where α is the angle between the outwards normal vector to the contour of integration and the crack direction, p_{x_i} and p_{y_i} are the components of stress vector in the i-th layer of the lower crack arm, u and v are the components of displacement vector with respect to the coordinate system xy (x is directed along the delamination crack), ds is a differential element along the contour of integration.

The components of J_{Γ_1} are expressed as

$$p_{x_i} = -\sigma_i,$$ (55)

$$p_{y_i} = 0,$$ (56)

$$ds = dz_1,$$ (57)

$$\cos\alpha = -1.$$ (58)

In (55), σ_i is determined by (8). The following formula from Mechanics of materials is applied to obtain the partial derivative, $\partial u / \partial x$, in (54):

$$\frac{\partial u}{\partial x} = \varepsilon = \varepsilon_{C_1} + \kappa_{y_1} y_1 + \kappa_{z_1} z_1.$$ (59)

The J-integral in segment, Γ_2, is written as

$$J_{\Gamma_2} = \sum_{i=1}^{i=n} \int_{z_{3i}}^{z_{3i+1}} \left[u_{0R_i} \cos\alpha_R - \left(p_{xR_i} \frac{\partial u}{\partial x_R} + p_{yR_i} \frac{\partial v}{\partial x_R} \right) \right] ds_R,$$ (60)

where

$$p_{xR_i} = \sigma_i,$$ (61)

$$p_{yR_i} = 0,$$ (62)

$$ds_R = -dz_3,$$ (63)

$$\cos\alpha_R = 1,$$ (64)

$$\frac{\partial u}{\partial x_R} = \varepsilon_R = \varepsilon_{C_3} + \kappa_{y_3} y_3 + \kappa_{z_3} z_3.$$ (65)

In (61), σ_i is obtained by (8) by replacing of ε with ε_R.

In segment, Γ_3, the J-integral is expressed as

$$J_{\Gamma_3} = \sum_{i=1}^{i=n_U} \int_{z_{2i}}^{z_{2i+1}} \left[u_{0U_i} \cos\alpha_U - \left(p_{xU_i} \frac{\partial u}{\partial x_U} + p_{yU_i} \frac{\partial v}{\partial x_U} \right) \right] ds_U,$$ (66)

where

$$p_{xU_i} = -\sigma_i,\qquad(67)$$

$$p_{yU_i} = 0,\qquad(68)$$

$$ds_U = dz_2,\qquad(69)$$

$$\cos\alpha_U = -1.\qquad(70)$$

$$\frac{\partial u}{\partial x_U} = \varepsilon_U = \varepsilon_{C_2} + \kappa_{y_2} y_2 + \kappa_{z_2} z_2.\qquad(71)$$

In (67), σ_i is obtained by (8) by replacing of ε with ε_U.

The average value of the J-integral along the delamination crack front is expressed as

$$J_{av} = \frac{1}{b}\int_{-\frac{b}{2}}^{\frac{b}{2}} J\,dy_1.\qquad(72)$$

Finally, by substituting of (53), (54), (60) and (66) in (72), one obtains

$$J_{av} = \frac{1}{b}\sum_{i=1}^{i=n_L}\int_{-\frac{b}{2}}^{\frac{b}{2}}\int_{z_{1i}}^{z_{1i+1}}\left[u_{0L_i}\cos\alpha - \left(p_{x_i}\frac{\partial u}{\partial x} + p_{y_i}\frac{\partial v}{\partial x}\right)\right]dy_1\,ds +$$

$$+\frac{1}{b}\sum_{i=1}^{i=n}\int_{-\frac{b}{2}}^{\frac{b}{2}}\int_{z_{3i}}^{z_{3i+1}}\left[u_{0R_i}\cos\alpha_R - \left(p_{xR_i}\frac{\partial u}{\partial x_R} + p_{yR_i}\frac{\partial v}{\partial x_R}\right)\right]dy_1\,ds_R +$$

$$+\frac{1}{b}\sum_{i=1}^{i=n_U}\int_{-\frac{b}{2}}^{\frac{b}{2}}\int_{z_{2i}}^{z_{2i+1}}\left[u_{0U_i}\cos\alpha_U - \left(p_{xU_i}\frac{\partial u}{\partial x_U} + p_{yU_i}\frac{\partial v}{\partial x_U}\right)\right]dy_1\,ds_U.\qquad(73)$$

The integration in (73) is carried-out by the MatLab computer program. The J-integral values obtained by (73) match the strain energy release rates calculated by (52). This fact proves the correctness of the delamination fracture analysis developed in the present paper.

3 Parametric Investigations

Parametric investigations of the delamination fracture are performed. The two three-layered functionally graded cantilever beam configurations shown in Fig. 4 are considered. A delamination crack is located between layers 2 and 3 in the beam configuration shown in Fig. 4a. A beam configuration with a delamination crack between layers 1 and 2 is also analyzed (Fig. 4b). The thickness of each layer is t_l. Calculations of the strain energy release rate are performed for both beam configurations (Fig. 4) by applying formula (52). The strain energy release rate is presented in non-dimensional form by using the formula $G_N = G/(q_{0_1}b)$. It is assumed that

$b = 0.025$ m, $t_l = 0.004$ m and $M = 50$ Nm. In order to evaluate the effect of the gradient of the material property, q_1, along the width of layer 1 on the delamination fracture behaviour, the strain energy release rate is plotted in non-dimensional form against p_{q_1} in Fig. 5 for both beam configurations shown in Fig. 4.
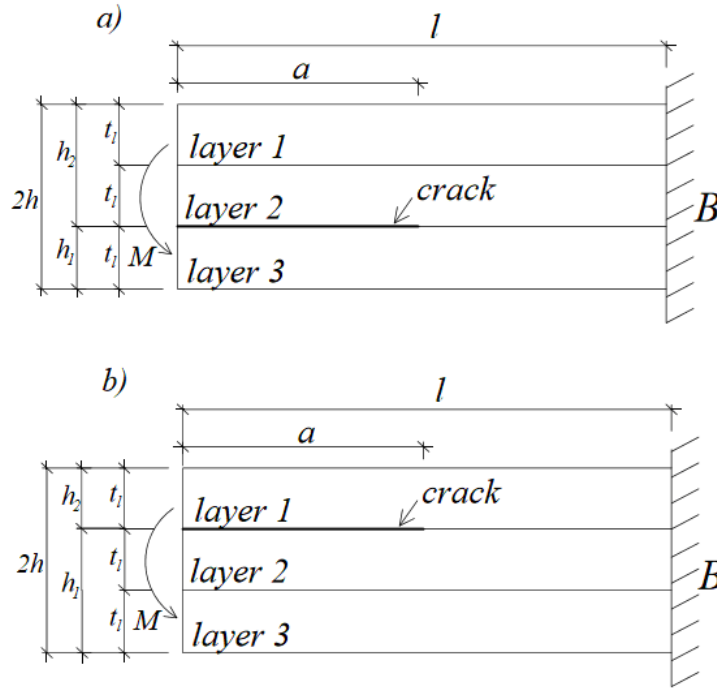

Figure 4: Two three-layered functionally graded beam configurations

It is assumed that $m_{q_1} = 1.7$, $p_{q_2} = 1.2$, $m_{q_2} = 1.3$, $q_{0_2}/q_{0_1} = 0.8$, $p_{q_3} = 1.4$, $m_{q_3} = 1.6$, $q_{0_3}/q_{0_1} = 1.7$, $p_{r_1} = 0.6$, $m_{r_1} = 0.5$, $r_{0_1}/q_{0_1} = 1.4$, $p_{r_2} = 0.6$, $m_{r_2} = 1.5$, $r_{0_2}/q_{0_1} = 0.8$, $p_{r_3} = 1.9$, $m_{r_3} = 0.8$ and $r_{0_3}/q_{0_1} = 2.2$. The curves in Fig. 5 indicate that the strain energy release rate increases with increasing of p_{q_1}. This behaviour is due to the fact that the beam stiffness decreases with increasing of p_{q_1}. The curves in Fig. 5 show also that the strain energy release rate increases when the delamination crack location changes from this shown in Fig. 4a to that shown in Fig. 4b.

The influence of the gradient of q_1 along the thickness of layer 1 on the strain energy release rate is also investigated. For this purpose, the strain energy release rate in non-dimensional form is presented as a function of m_{q_1} in Fig. 6. The three-layered functionally graded beam configuration with a delamination crack located between layers 1 and 2 (Fig. 4b) is analyzed. It is assumed that $p_{q_1} = 0.6$, $p_{q_2} = 1.2$, $m_{q_2} = 1.3$, $q_{0_2}/q_{0_1} = 0.8$, $p_{q_3} = 1.4$, $m_{q_3} = 1.6$, $q_{0_3}/q_{0_1} = 1.7$, $p_{r_1} = 0.6$, $m_{r_1} = 0.5$, $r_{0_1}/q_{0_1} = 1.4$, $p_{r_2} = 0.6$, $m_{r_2} = 1.5$, $r_{0_2}/q_{0_1} = 0.8$, $p_{r_3} = 1.9$, $m_{r_3} = 0.8$ and $r_{0_3}/q_{0_1} = 2.2$. One can observe in Fig. 6 that the strain energy release rate increases with increasing of m_{q_1}. The effect of the non-linear mechanical behaviour of the functionally graded material on the strain energy release rate is evaluated too. The three-layered functionally graded beam configuration shown in Fig. 4b is considered. The strain energy release rate derived assuming linear-elastic behaviour of the functionally graded material is plotted in non-dimensional form against m_{q_1} in Fig. 6 for comparison with the non-linear solution. It should be noted that the linear-elastic solution for the strain energy release rate is derived by substituting of $r_{0_i} = 0$ in formula (52). It can be observed in Fig. 6 that the non-linear behaviour of the functionally graded material leads to increase of the strain energy release rate.
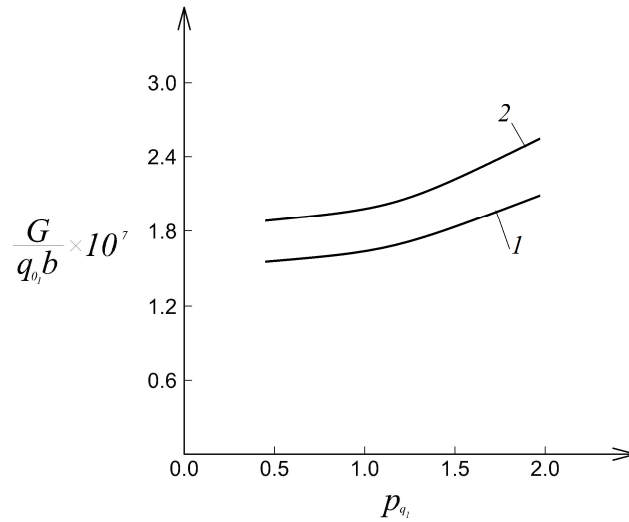
Figure 5: The strain energy release rate in non-dimensional form presented as a function of material property, p_{q_1}, for the three-layered functionally graded beam containing a crack between layers 2 and 3 (curve 1) and the three-layered functionally graded beam containing a crack between layers 1 and 2 (curve 2)

The influence of the gradients of the material property, r_1, along the width as well as along the thickness of layer 1 on the strain energy release rate is also explored.
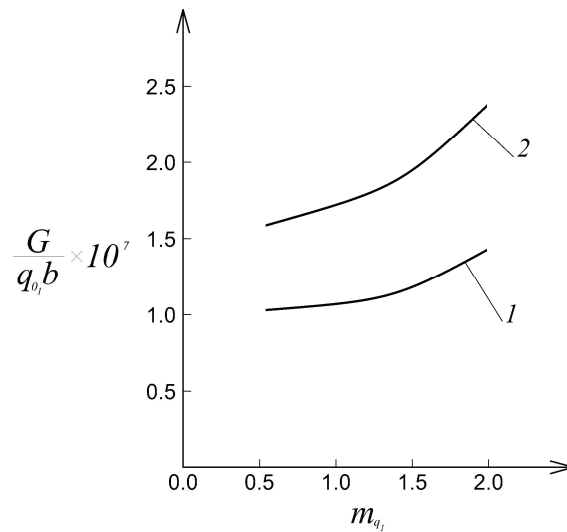

Figure 6: The strain energy release rate in non-dimensional form presented as a function of material property, m_{q_1}, at linear-elastic behaviour of the functionally graded material (curve 1) and non-linear behaviour of the functionally graded material (curve 2)

For this purpose, the strain energy release in non-dimensional form is presented as a function of p_{r_1} in Fig. 7 at three values of m_{r_1}.
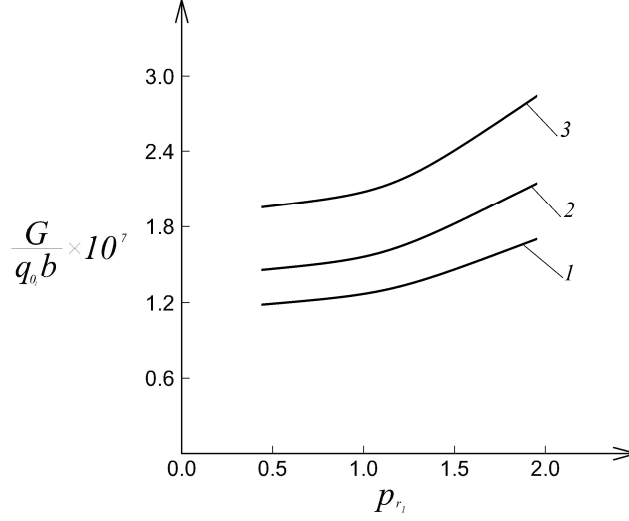
216

Figure 7: The strain energy release rate in non-dimensional form presented as a function of material property, p_{r_1}, at $m_{r_1} = 0.5$ (curve 1), $m_{r_1} = 0.7$ (curve 2) and $m_{r_1} = 1.2$ (curve 3)

The three-layered functionally graded beam configuration with a delamination crack between layers 1 and 2 (Fig. 4b) is considered. It is assumed that $p_{q_1} = 0.6$, $m_{q_1} = 0.7$, $p_{q_2} = 1.2$, $m_{q_2} = 1.3$, $q_{0_2}/q_{0_1} = 0.8$, $p_{q_3} = 1.4$, $m_{q_3} = 1.6$, $q_{0_3}/q_{0_1} = 1.7$, $r_{0_1}/q_{0_1} = 1.4$, $p_{r_2} = 0.6$, $m_{r_2} = 1.5$, $r_{0_2}/q_{0_1} = 0.8$, $p_{r_3} = 1.9$, $m_{r_3} = 0.8$ and $r_{0_3}/q_{0_1} = 2.2$. The curves in Fig. 7 show that the strain energy release rate increases with increasing of p_{r_1} and m_{r_1}.

4   Conclusions

The delamination fracture in multilayered functionally graded cantilever beam configuration is analyzed with taking into account the non-linear mechanical behaviour of the material. It is assumed that the material in each layer is functionally graded in both width and thickness directions. The non-linear behaviour of the functionally graded material is described by using a stress-strain relation that involves two material properties. Logarithmic laws are applied to describe the continuous variation of the two material properties in the cross-sections of the layers. It should be mentioned that the material properties are distributed non-symmetrically with respect to the centroidal axes of the beam cross-section. A solution for the strain energy release rate is derived by considering the balance of the energy. A comparison with the *J*-integral approach is performed for verification. The solution obtained is applicable for beams made of an arbitrary number of functionally graded layers which have different thicknesses and material properties. Parametric investigations of the delamination fracture behaviour are carried-out. Two three-layered functionally graded beam configurations are considered in order to evaluate the effect of the crack location along the beam height. It is found that the strain energy release rate increases when the material properties, p_{q_1} and m_{q_1}, increase (p_{q_1} and m_{q_1} govern the gradients of the material property, q_1, in the width and thickness directions of layer 1, respectively). The analysis reveals also that the strain energy release rate increases with increasing of p_{r_1} and m_{r_1} (p_{r_1} and m_{r_1} govern the gradients of the material property, r_1, in the width and thickness directions of layer 1, respectively). The results obtained in the present paper show that the strain energy release rate can be controlled by employing materials with appropriate two-dimensional gradients in the design stage of the multilayered functionally graded non-linear elastic structural members and components.

217

References

Broek, D.: *Elementary engineering fracture mechanics*. Springer (1986).

Bykov, Yu. V.; Egorov, S. V.; Ermeev, A. G.; Holoptsev, V. V.: Fabrication of metal-ceramic functionally graded materials by microwave sintering. *Inorganic Materials: Applied Research*, 3, (2012), DOI: 10.1134/S20751133120300057.

Dowling, N.: *Mechanical Behavior of Materials*. Pearson (2007).

Dolgov, N.A.: Determination of Stresses in a Two-Layer Coating. *Strength of Materials* 37, (2005), 422-431.

Dolgov, N.A.: Analytical Methods to Determine the Stress State in the Substrate–Coating System Under Mechanical Loads. *Strength of Materials* 48, (2016), 658-667.

Farris, T.N.; Doyle, J.F.: A global/local approach to lengthwise cracked beams: static analysis. *International Journal of Fracture*, 50, (1991), 131-141.

Gasik, M.M.: Functionally graded materials: bulk processing techniques. *International Journal of Materials and Product Technology*, 39, (2010), 20-29.

Hirai, T.; Chen, L.: Recent and prospective development of functionally graded materials in Japan. *Mater Sci. Forum*, 308-311, (1999), 509-514.

Hsueh, C.H.; Tuan, W.H.; Wei, W.C.J.: Analyses of steady-state interface fracture of elastic multilayered beams under four-point bending. *Scripta Mater*, 60, (2009), 721 - 724.

Kienzler, R.; Herrmann, G.: Configurational Mechanics Applied to Strength of Materials. In: Kienzler R., Maugin G.A. (eds), *Configurational Mechanics of Materials*. International Centre for Mechanical Sciences (Courses and Lectures), 427, (2001), Springer, Vienna.

Kienzler, R.: Bose, D.K.: Material Conservation Laws Established Within a Consistent Plate Theorie. In: Jaiani G., Podio-Guidugli P. (eds) IUTAM Symposium on Relations of Shell Plate Beam and 3D Models. *IUTAM Bookseries*, 9, (2008), Springer, Dordrecht.

Lukash, P.A.: *Fundamentals of non-linear structural mechanics*. Stroizdat (1998).

Mortensen, A.; Suresh, S.: Functionally graded metals and metal-ceramic composites: Part 1 Processing. *Int. Mater. Rev*., 40, (1995), 239-265.

Nemat-Allal, M.M.; Ata, M.H.; Bayoumi, M.R,; Khair-Eldeen, W.: Powder metallurgical fabrication and microstructural investigations of Aluminum/Steel functionally graded material. *Materials Sciences and Applications*, 2, (2011), 1708-1718.

Neubrand, A.; Rödel, J.: Gradient materials: An overview of a novel concept. *Zeit. f. Met*., 88, (1997), 358-371.

Rizov, V.: Delamination of Multilayered Functionally Graded Beams with Material Nonlinearity. *International Journal of Structural Stability and Dynamics*, (2017), doi.org/10.1142/S0219455418500517.

Schneider, P.; Kienzler, R.: An Algorithm for the Automatisation of Pseudo Reductions of PDE Systems Arising from the Uniform-approximation Technique. In: Altenbach H., Eremeyev V. (eds), *Shell-like Structures. Advanced Structured Materials*, 15, (2011), Springer, Berlin, Heidelberg.

Suresh, S.; Mortensen, A.: *Fundamentals of functionally graded materials*. London: IOM Communications Ltd (1998).

Szekrenyes, A.: Semi-layerwise analysis of laminated plates with nonsingular delamination-The theorem of autocontinuity. *Applied mathematical modelling*, 40, (2016), 1344 – 1371.

Szekrenyes, A.: Nonsingular crack modelling in orthotropic plates by four equivalent single layers. *European journal of mechanics – A/solids*, 55, (2016), 73-99.

Upadhyay, A.K.; Simha, K.R.Y.: Equivalent homogeneous variable depth beams for cracked FGM beams; compliance approach. *Int. J. Fract.*, 144, (2007), 209-213.

Uslu Uysal, M.; Kremzer, M.: Buckling Behaviour of Short Cylindrical Functionally Gradient Polymeric Materials. *Acta Physica Polonica A*, 127, (2015), 1355-1357, DOI:10.12693/APhysPolA.127.1355.

Uslu Uysal, M.: Buckling behaviours of functionally graded polymeric thin-walled hemispherical shells. *Steel and Composite Structures, An International Journal*, 21, (2016), 849-862.

Uslu Uysal, M.; Güven, U.: A Bonded Plate Having Orthotropic Inclusion in Adhesive Layer under In-Plane Shear Loading. *The Journal of Adhesion*, 92, (2016), 214-235, DOI:10.1080/00218464.2015.1019064.

Yan, T. ; Yang, J.: Forced vibration of edge-cracked functionally graded beams due to a transverse moving load. *Procedia Engineering*, 14, (2011), 3293-3300.

Address: Prof. Dr. Victor Rizov, Department of Technical Mechanics, University of Architecture, Civil Engineering and Geodesy, 1 Chr. Smirnensky blvd., 1046 – Sofia, Bulgaria
email: V_RIZOV_FHE@UACG.BG